A Multi-Scale Computational Approach to Understanding Cancer Metabolism

Angelo Lucia and Peter A. DiMaggio

This chapter is divided into two parts. In the first part, an overview of the Nash equilibrium approach to metabolic pathway modeling, simulation, and analysis is presented, showing the reader the basic formulations and key modeling considerations. Small examples are used to elucidate key ideas, including the explicit use of enzyme reactions, up-/downregulation of enzymes, and allosteric inhibition. In the second part of this chapter, the Nash equilibrium approach is applied to the methionine salvage pathway (MSP) to highlight the predictive capabilities of the approach and to help in building an understanding of cancer metabolism. Experimental data is used to validate the proposed Nash equilibrium MSP model.

1 The Fundamentals of Nash Equilibrium and Metabolic Pathway Analysis

A rigorous, multi-scale Nash equilibrium model based on first principles (i.e., chemical reaction equilibrium thermodynamics and element mass balancing) is presented.

A. Lucia (✉)
Department of Chemical Engineering, University of Rhode Island, Kingston, RI, USA
e-mail: alucia@uri.edu

P. A. DiMaggio
Department of Chemical Engineering, Imperial College London, London, UK
e-mail: p.dimaggio@imperial.ac.uk

S. Consoli et al. (eds.), *Data Science for Healthcare*,
https://doi.org/10.1007/978-3-030-05249-2_13

1.1 Introduction

In recent work, Lucia, DiMaggio, and co-workers [1–3] have introduced the idea of treating metabolic pathways as Nash equilibria using first principles (i.e., rigorous chemical reaction equilibrium and elemental mass balancing involving charged and electrically neutral species). The key ideas behind the Nash equilibrium approach to metabolic pathway analysis are as follows:

1. Enzymes are players in a multi-player game.
2. The objective or payoff function for each player results in a constrained nonlinear programming (NLP) problem. That is, each player (enzyme) minimizes the Gibbs free energy of the reaction it catalyzes subject to element mass balances.
3. The goal of the metabolic network is to find the best overall solution given the natural competition for nutrients among enzymes.

The Nash equilibrium approach has many advantages over methods such as flux balance analysis (FBA) and its many variants, constraint-based modeling (CBM), and kinetic approaches to determining fluxes and other information throughout a metabolic network. More specifically, treating any metabolic pathway as a Nash equilibrium allows one to:

1. include co-factors in modeling sub-networks.
2. model electrolyte solution behavior and incorporate charge balancing.
3. include feedback, allosteric, and other forms of inhibition.
4. explicitly include enzyme-substrate reactions as part of the model.
5. upscale genetic information and consider mutations and/or re-engineered enzymes.
6. model up-/downregulation of enzymes.

Modeling metabolic pathways using Nash equilibrium is purely predictive and to date has been used to model a number of common pathways including glycolysis, the Krebs cycle, acetone-butanol-ethanol (ABE) production, and the mevalonate pathway. In cases where experimental data are available, numerical predictions, to date, show remarkably good agreement with experimental metabolite concentrations and other biological metrics such as turnover number.

1.2 Nash Equilibrium Formulation of a Metabolic Network

In this section, the basic Nash equilibrium formulation for metabolic pathway analysis is described. Metabolite, co-factor, and enzyme-substrate reactions are included. Simple illustrative examples are presented to make key ideas clear to the reader.

Let the unknown variables, v, be partitioned into N subsets, $v = [v_1, v_2, \ldots, v_N]$, in which each variable partition, v_j, has n_j unknown variables.

While the FBA formulation for metabolic pathway analysis is a linear program with an arbitrary objective not based in first principles, the Nash equilibrium (NE) formulation for an arbitrary metabolic network is quite different and is given by a collection of $j = 1, 2, \ldots, N$ nonlinear programming (NLP) sub-problems of the form

$$\begin{array}{ll} \min & \frac{G_j(v_j)}{RT} \\ \text{subject to} & \text{conservation of mass} \\ & v^*_{-j} \end{array} \tag{1}$$

where $\frac{G_j}{RT}$, the dimensionless Gibbs free energy, is the objective function associated with the appropriate enzyme that catalyzes one or more reactions at a given node j in the network, R is the universal gas constant, and T is the temperature. The conservation of mass constraints are elemental mass balances and can involve *charged* species, and v_j represents the flux of metabolic material in and out of any node. Finally, the vector, v^*_{-j}, denotes the minima of all *other* sub-problems, $k = 1, 2, \ldots, j-1, j+1, \ldots, N$. In this chapter sub-problem and node mean the same thing. The Gibbs free energy for sub-problem j is given by

$$\frac{G_j}{RT} = \sum_{i=1}^{C_j} x_{ij} \left[\frac{\Delta G^0_{ij}}{RT} + \ln x_{ij} + \ln \phi_{ij} \right] \tag{2}$$

where ΔG^0_{ij} are the standard Gibbs free energies of reaction at 25 °C for the metabolic reactions associated with sub-problem j, x_{ij} are mole fractions which are related to the fluxes, ϕ_{ij} are fugacity coefficients, i is a component index, and C_j and R_j are the number of components and number of reactions associated with a sub-problem j in the network. For example, it is not uncommon to have coupled metabolite and co-factor reactions at a given node.

Temperature effects in the NE formulation are taken into account using the van't Hoff equation, which is given by

$$\frac{\Delta G^0_{ij}(T)}{RT} = \frac{\Delta G^0_{ij}(T_0)}{RT_0} + \frac{\Delta H^0_{ij}(T_0)}{R} \left[\frac{T - T_0}{T T_0} \right] \tag{3}$$

where T_0 is the reference temperature (usually 25 °C), T is the temperature at which the reaction takes place (usually 37 °C), and $\Delta H^0_{ij}(T_0)$ is the standard enthalpy change of reaction i at node j in the network. All standard Gibbs free energy changes due to reaction, $\Delta G^{R0}_{ij}(T_0)$, and the enthalpy changes due to reaction, $\Delta H^{R0}_{ij}(T_0)$, can be computed from Gibbs free energies and enthalpies of formation and reaction stoichiometry

$$\Delta G^{R0}_{ij} = \sum_{k=1}^{n_p(ij)} s_k \Delta G^0_{f,ijk} - \sum_{k=1}^{n_r(ij)} s_k \Delta G^0_{f,ijk} \tag{4}$$

where the s_k's are the stoichiometric numbers and $n_p(ij)$ and $n_r(ij)$ are the number of products and number of reactants, respectively, associated with reaction i and node j. The Gibbs free energy of formation data for metabolites and co-factors used in this chapter can be found on the eQuilibrator website (http://equilibrator.weizmann.ac.il/). Enzyme-substrate binding energies can be found in Appendix 1.

The network objective is given by

$$\frac{G(v)}{RT} = \sum_{j=1}^{N} \min \frac{G_j(v_j)}{RT} \tag{5}$$

The key attribute that distinguishes the proposed NE approach from other formulations and makes the problem challenging is that the objective functions in all sub-problems are nonlinear.

1.3 Metabolite/Co-factor Reactions, Mass, and Charge Balances

Most biological reactions involve metabolites, co-factors, and enzymes. Element mass balances in the Nash equilibrium formulation are written in the following matrix-vector form

$$Av = b \tag{6}$$

and correct element mass balancing guarantees that charge balances will be satisfied.

Illustrative Example 1: Mass and Charge Balancing Consider the example of the dehydration of S-methyl-5-thio-D-ribulose 1-phosphate (MTRu-1P) to form 2,3-diketo-5-methylthiopentyl-1-phosphate (DK-MTP-1P) and water. The chemical reaction is

$$C_6H_{11}O_7PS^{-2} \rightleftharpoons C_6H_9O_6PS^{-2} + H_2O \tag{7}$$

which is balanced, both with respect to elemental masses (i.e., carbon, hydrogen, oxygen, phosphorous, and sulfur) and electrical charge. The element mass balances for all species involved in this reaction are

$$\begin{pmatrix} 2 & 11 & 9 \\ 1 & 7 & 6 \\ 0 & 6 & 6 \\ 0 & 1 & 1 \\ 0 & 1 & 1 \end{pmatrix} \begin{pmatrix} v_{H_2O} \\ v_{MTRu\text{-}1P} \\ v_{DK\text{-}MTP\text{-}1P} \end{pmatrix} = \begin{pmatrix} H \\ O \\ C \\ P \\ S \end{pmatrix} \quad \begin{matrix} \text{hydrogen} \\ \text{oxygen} \\ \text{carbon} \\ \text{phosphorous} \\ \text{sulfur} \end{matrix} \tag{8}$$

Table 1 Minimum Gibbs free energy solution for MTRu-1P $\rightleftharpoons$ DK-MTP-1P + H_2O

Species	Initial metabolic pool (nmols)	Equilibrium fluxes (nmol/s)
Water	0.84073	0.84076
MTRu-1P	0.07226	0.07207
DK-MTP-1P	0.08702	0.08718

However, element mass balances must be linearly independent; otherwise numerical difficulties can arise. First note that rows 3, 4, and 5 in Eq. (8) are linearly dependent because carbon, phosphorous, and sulfur are in the same ratio (6:1:1) in MTRu-1P and DK-MTP-1P and are absent from water. Next, note that the sum of columns 1 and 3 is linearly dependent with column 2 and thus the matrix has column rank of 2. Since row and column rank of any matrix must be equal, this means that only two element mass balances can be linearly independent.

Illustrative Example 2: Linearly Independent Constraints In the previous illustration, the correct choice of linearly independent mass balances is hydrogen and oxygen. This choice is based on the fact that only hydrogen and oxygen are transferred from MTRu-1P during dehydration. Equation (9) gives the correct linearly independent constraints for converting MTRu-1P to DK-MTP-1P and water; the resulting minimum Gibbs free energy (equilibrium) solution is shown in Table 1.

$$\begin{pmatrix} 2 & 11 & 9 \\ 1 & 7 & 6 \end{pmatrix} \begin{pmatrix} \upsilon_{H_2O} \\ \upsilon_{\text{MTRu-1P}} \\ \upsilon_{\text{DK-MTP-1P}} \end{pmatrix} = \begin{pmatrix} \text{H} \\ \text{O} \end{pmatrix} = \begin{pmatrix} 3.25933 \\ 1.86857 \end{pmatrix} \quad \begin{matrix} \text{hydrogen} \\ \text{oxygen} \end{matrix} \tag{9}$$

1.4 Enzymatic Reactions

The general reaction sequence for enzyme-substrate reactions is

$$\text{E} + \text{S} \rightleftharpoons \text{E} - \text{S} \qquad \text{(binding)} \tag{10}$$

$$\text{E} - \text{S} \rightleftharpoons \text{E} + \text{P} \qquad \text{(unbinding)} \tag{11}$$

where E, S, E − S, and P denote enzyme, substrate, enzyme-substrate complex, and product, respectively. Enzyme-substrate reactions can be included in the Nash

equilibrium framework in much the same way as metabolite and co-factor reactions with two key assumptions:

1. Enzymes may have charged fragments but have no net charge.
2. There is no mass transfer of carbon, hydrogen, etc. to or from enzymes. These assumptions result in the following mass balances for single binding and unbinding events between an enzyme, a substrate, and a product

$$\begin{pmatrix} a_{11} & 0 & a_{12} \\ 0 & 1 & 1 \end{pmatrix} \begin{pmatrix} v_{\mathrm{M}} \\ v_{\mathrm{E}} \\ v_{\mathrm{C}} \end{pmatrix} = \begin{pmatrix} \mathrm{M} \\ \mathrm{E} \end{pmatrix} \tag{12}$$

where the subscripts M, E, and C in Eq. (12) denote metabolites (substrate or product), enzyme, and enzyme complex (i.e., E − S), respectively, and M and E on the right-hand side are molar amounts of metabolite and enzyme, respectively.

Illustrative Example 3: Including Enzymes To illustrate, consider the conversion of oxaloacetate and acetyl CoA to citrate and co-enzyme A by the enzyme E = citrate synthase, which is the first step in the tricarboxylic acid (Krebs) cycle. The reaction sequence consists of two binding reactions, the main reaction and then one unbinding reaction, and is given by

$$\mathrm{E} + \mathrm{C_4H_2O_5^{-2}} \rightleftharpoons \mathrm{E - C_4H_2O_5^{-2}} \quad \text{(binding of oxaloacetate)} \tag{13}$$

$$\mathrm{E} + \mathrm{C_{23}H_{34}N_7O_{17}P_3S^{-4}} \rightleftharpoons \mathrm{E - C_{23}H_{34}N_7O_{17}P_3S^{-4}} \quad \text{(binding of acetyl CoA)} \tag{14}$$

$$\mathrm{E - C_4H_2O_5^{-2}} + \mathrm{E - C_{23}H_{34}N_7O_{17}P_3S^{-4}} + \mathrm{H_2O} \rightleftharpoons \mathrm{E} + \mathrm{C_6H_5O_7^{-3}} + \mathrm{C_{21}H_{32}N_7O_{16}P_3S^{-4}} + \mathrm{H^+} \quad \text{(unbinding of citrate } \textit{and} \text{ CoA)} \tag{15}$$

There are five linearly independent element mass balances and six fluxes in this example, as shown below:

$$\begin{pmatrix} 2 & 32 & 5 & 0 & 2 & 34 \\ 0 & 7 & 0 & 0 & 0 & 7 \\ 1 & 16 & 7 & 0 & 5 & 17 \\ 0 & 21 & 6 & 0 & 4 & 23 \\ 0 & 0 & 0 & 1 & 1 & 1 \end{pmatrix} \begin{pmatrix} v_{\mathrm{H_2O}} \\ v_{\mathrm{CoA}} \\ v_{\mathrm{citrate}} \\ v_{\mathrm{E}} \\ v_{\mathrm{E\text{-}AcCoA}} \\ v_{\mathrm{E\text{-}oxalo}} \end{pmatrix} = \begin{pmatrix} \mathrm{H} \\ \mathrm{N} \\ \mathrm{O} \\ \mathrm{C} \\ \mathrm{E} \end{pmatrix} \tag{16}$$

Table 2 gives numerical results for an initial metabolic pool containing 0.5 μM oxaloacetate and acetyl CoA plus 0.05 μM native citrate synthase (PDB # 4G6B).

1.5 Up-/Downregulation of Enzymes

The amounts of proteins (enzymes) in a cell are usually controlled by gene regulation in response to internal or external factors (e.g., a drug). The net result is either an increase (upregulation) or decrease (downregulation) of the amount of protein (or protein expression). It is straightforward to study the impact of up-/downregulation of enzymes in the Nash equilibrium framework by simply increasing/decreasing the amount of enzyme in the initial metabolic pool.

Illustrative Example 4: Upregulation of Citrate Synthase To illustrate upregulation, consider the impact of increasing the amount of citrate synthase in the metabolic pool in Table 2 from 0.0001 to 0.00015 nmols while keeping all metabolite concentrations fixed. A comparison of the equilibrium concentrations for nominal (0.0001 nmols) and upregulated (0.00015 nmols) amounts of citrate synthase is shown in Table 2. Note that the model predictions are at the very least qualitatively correct. Increasing the amount of enzyme results in a decrease in the equilibrium concentrations of reactants and an increase in the equilibrium concentrations of products. More specifically, the concentrations of citrate and co-enzyme A increase by ∼5%. In addition, all enzyme complexes increase in concentration.

1.6 Allosteric Inhibition

It is well known that the co-factor NADH is a strong allosteric inhibitor of citrate synthase. In fact, Yim et al. [4] describe a specific genetically engineered mutation (PDB # 1OWB) used in the production of 1,4-butanediol from *E. coli* that significantly reduces NADH inhibition of citrate synthase. The specific genetic modification used by Yim et al. has leucine in place of arginine on residue 163 of the enzyme.

Illustrative Example 5: Allosteric Inhibition Continuing with the behavior of citrate synthase, consider the nominal metabolic pool shown in Table 2, which in this illustration contains 0.0001 nmols of citrate synthase and 0.001 nmols of NADH. If the Nash equilibrium approach correctly captures allosteric inhibition, then the concentrations of citrate and co-enzyme A produced should decrease in the presence of NADH. A comparison of the third column from the right with the last column of Table 2 bears this out. Citrate and co-enzyme A concentrations decrease by 84.4%. Note also that the equilibrium concentration of free citrate synthase available for catalysis is reduced by 7% while the binding of NADH to the enzyme is significant.

Table 2 Equilibrium concentrations for citrate production: citrate synthase (4G6B)

Species	Metabolic pool (nmols)	Nominal (μM)	Upregulated (μM)	Inhibited (μM)
Oxaloacetate	0.0001	0.342912	0.331124	0.526544
Acetyl CoA	0.0001	0.289517	0.289517	0.289517
Citrate synthase (E)	0.0001, 0.00015	4.08927	4.10640	3.80270
E-oxaloacetate		0.133417	0.126567	0.248045
E-acetyl CoA		0.012089	0.013603	∼0
Citrate		0.181155	0.190287	0.028317
Co-enzyme A		0.135866	0.142715	0.021237
NADH	0.001			4.68262
E-NADH				0.905379

Table 3 Impact on equilibrium concentrations from genetic modification of citrate synthase inhibition

Species	Metabolic pool (nmols)	PDB # 4G6B (μM)	PDB # 1OWB (μM)
Oxaloacetate	0.0001	0.526544	0.517328
Acetyl CoA	0.0001	0.289517	0.289518
Citrate synthase (E)	0.0001	3.80270	3.18897
E-oxaloacetate		0.248045	0.241539
E-acetyl CoA		∼0	∼0
Citrate		0.028317	0.036991
Co-enzyme A		0.021237	0.027744
NADH	0.001	4.68262	5.64453
E-NADH		0.905379	0.143040

Both of these facts clearly show that NADH inhibits the conversion of oxaloacetate and acetyl CoA to citrate and CoA.

Illustrative Example 6: Genetic Modification To illustrate that the Nash equilibrium approach captures the impact of genetic modification, the previous illustration is re-solved by replacing the native citrate synthase structure (PDB # 4G6B) with the re-engineered structure (PDB # 1OWB) used by Yim et al. [4]. Table 3 shows a comparison of the equilibrium concentrations that are predicted for both citrate synthase structures, PDB # 4G6B and 1OWB.

Note that the re-engineered citrate synthase structure (PDB # 1OWB) results in a significant increase in the equilibrium concentrations of citrate and co-enzyme A of ∼30% and a decrease in the equilibrium concentrations of the reactants oxaloacetate and acetyl CoA when compared to the native structure (PDB # 4G6B). Moreover, the amount of NADH bound to the enzyme is reduced by 84%, and this, in turn, results in an increase in the equilibrium concentration of citrate synthase available for converting oxaloacetate and acetyl CoA to citrate and CoA.

2 Understanding Cancer Metabolism: The Methionine Salvage Pathway

Methionine is an essential amino acid that cannot be produced de novo in mammals and must be ingested through food and/or supplementation. *S*-Adenosyl methionine (SAM) is a derivative of methionine and serves as a methyl donor group for methylation of DNA, RNA, and proteins such as histones. The methionine salvage pathway and the associated metabolites and co-factors are important in understanding cancer metabolism. Key among those metabolites and co-factors are methionine, SAM, methylthioadenosine (MTA), and S-methyl-5-thio-D-ribose (MTR-1P). The methionine salvage pathway is shown in Fig. 1, and the corresponding biochemical reactions are given in Appendix 2.

It is now well established that the gene encoding S-methyl-5′-thioadenosine phosphorylase (MTAP), the enzyme that converts MTA to MTR-1P in the methionine salvage pathway, is often co-deleted in many types of cancers (e.g., glioblastoma, leukemia, lung, lymphoma, mesothelioma, osteosarcoma, pancreatic) since it is adjacent to the tumor suppressor CDKN2a on the chromosome 9p21 locus [6]. While this deletion affects methionine metabolism by effectively eliminating the methionine salvage pathway, it also leads to an accumulation of MTA, which

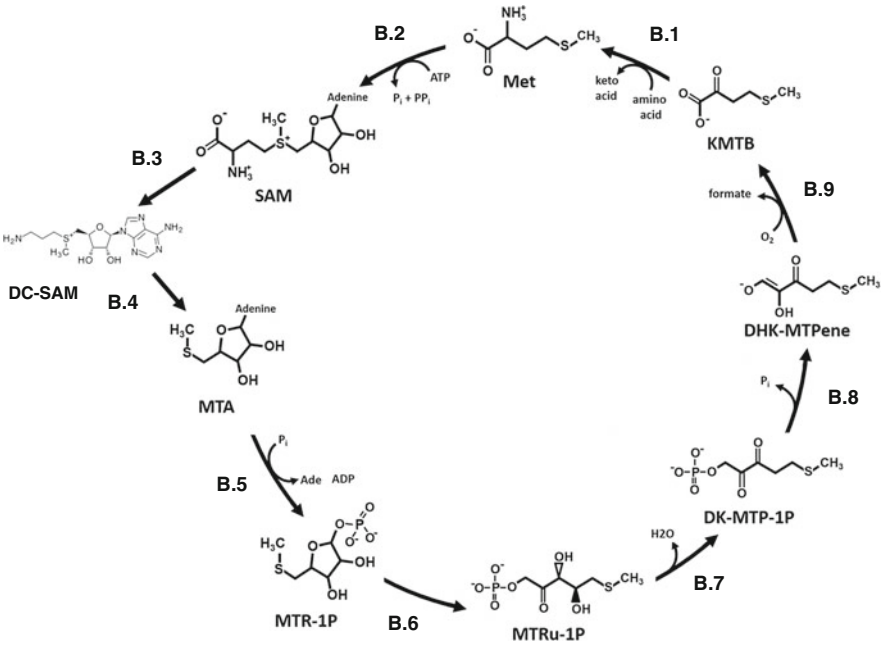

Fig. 1 Methionine salvage pathway adapted from [5]. The complete set of biochemical reactions are provided in Appendix 2

is toxic to cells due to feedback inhibition of spermidine synthase. Recent work by Kirovski et al. [7] and Chang et al. [8] has also shown that other types of cancer cells, such as hepatocellular carcinoma (HCC), exhibit loss of MTAP activity resulting from hyper-methylation of its gene promoter, and this also leads to accumulation of intracellular MTA. Additionally, Kamatani and Carlson [9] provide evidence that increased levels of MTA result in increased concentration of putrescine but inhibit spermidine synthetase. Finally, attempts to inhibit MTAP in order to starve cancer cells of SAM and kill them have only met with marginal success [8], showing only slight improvement in prolonging life in cancer patients.

2.1 Baseline Simulations of the Methionine Salvage Pathway

To provide some basis for comparison, baseline steady-state equilibrium concentrations for the methionine salvage pathway for a model consisting of metabolite/co-factor-only reactions were computed using the Nash equilibrium approach. Two separate initial pools were used—one corresponding to very low methionine (or a vegan diet) and the other to normal levels of methionine (or a diet consisting of meat and dairy). The primary interest here is to determine if the Nash equilibrium approach can provide good quantitative predictions of equilibrium concentrations in the physiological range.

Table 4 gives results for two separate initial metabolic pools containing some, but not all, metabolites. Note that all metabolite concentrations fall within the normal physiological range and in some cases match almost perfectly with experimentally reported values in Table 4, particularly for the normal methionine diet.

As mentioned above, the amount of intracellular methionine is primarily dependent upon the available food source. Early work by Eagle [17] identified 100 μM as a suitable concentration of methionine for culturing mammalian cells and is currently used in several media formulations (e.g., RPMI, MEM). Recent studies have shown that concentrations of methionine above 25 μM are required for cell proliferation [10] as well as maintenance and growth of undifferentiated stem cells [11]. The equilibrium methionine concentrations predicted by the Nash equilibrium approach based entirely on first principles fall within the physiological range and are impressively close to reported experimental values, as shown in Fig. 2. Similarly, the equilibrium concentrations predicted for SAM and MTA by the Nash equilibrium approach are remarkably close to reported experimental values from a variety of sources, as shown in Table 4. As discussed in [14], the impact of MTA concentrations on tumor cells remains a controversial topic since [0.5–5] μM MTA reportedly promotes tumor progression while higher concentrations have been found to impede cell proliferation and tumor development, so this has been referenced as an upper bound in MTA concentration.

It is important to note that there are several other studies that report the intracellular concentrations for SAM and MTA on a relative basis such as nmol per million cells or per mg of protein. However, these values cannot be used as absolute

Table 4 Methionine salvage pathway baseline equilibrium concentrations starting from an initial metabolite pool (nmol) of 0.2 glutamate, 1 water, 2 ATP, 1 H^+, 0.05 putrescine, 0.075 MTA, 1 O_2, 1 KMTB

Species	NE Conc 1 (μM)	NE Conc 2 (μM)	Experimental (μM)	References
Initial Met pool[a]	34.92	69.84		
Methionine (Met)	57.97	108.00	>25	[10]
				[11]
			83.6	[11]
SAM	35.45	42.31	59	[12]
			46.2	[11]
			50	[13]
MTA	0.23	0.23	0.264	[11]
			<5	[14]
Putrescine	0.38	0.39	[0.05, 0.3]	[15]
ATP	1325	1319	[1290, 1790]	[15]
Adenine[b]	2.10	2.10	[0.5, 3]	[16]

[a]Corresponds to 0.005 and 0.1 nmols in initial pool
[b]Adenine is regulated at 0.003 nmols in metabolite pool; regulation results in 0.123 nmols of adenine output

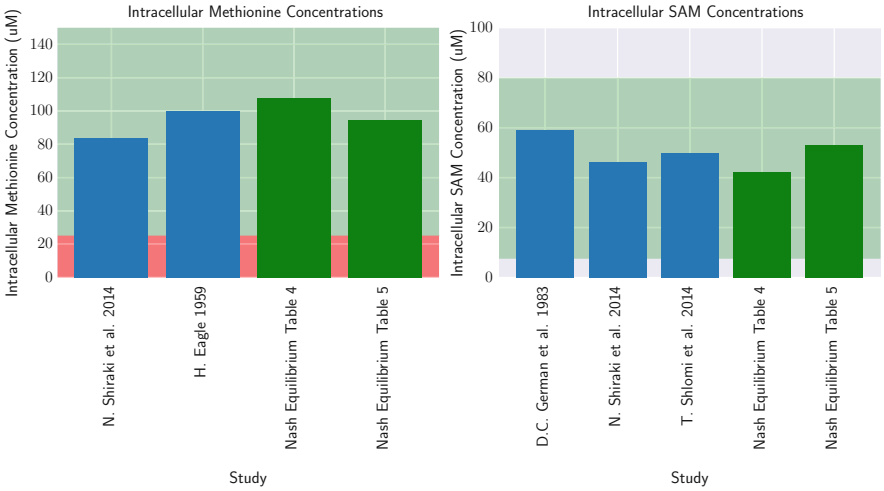

Fig. 2 Comparison between experimental and predicted intracellular concentrations for methionine and SAM

quantities since they are found to differ by several orders of magnitude between sources and even between studies performed by the same authors. While such values cannot be used to infer absolute concentrations, they are useful for computing relative concentrations between metabolites that were measured by the same assay. Figure 3 presents the ratios in concentrations for methionine/SAM and SAM/MTA

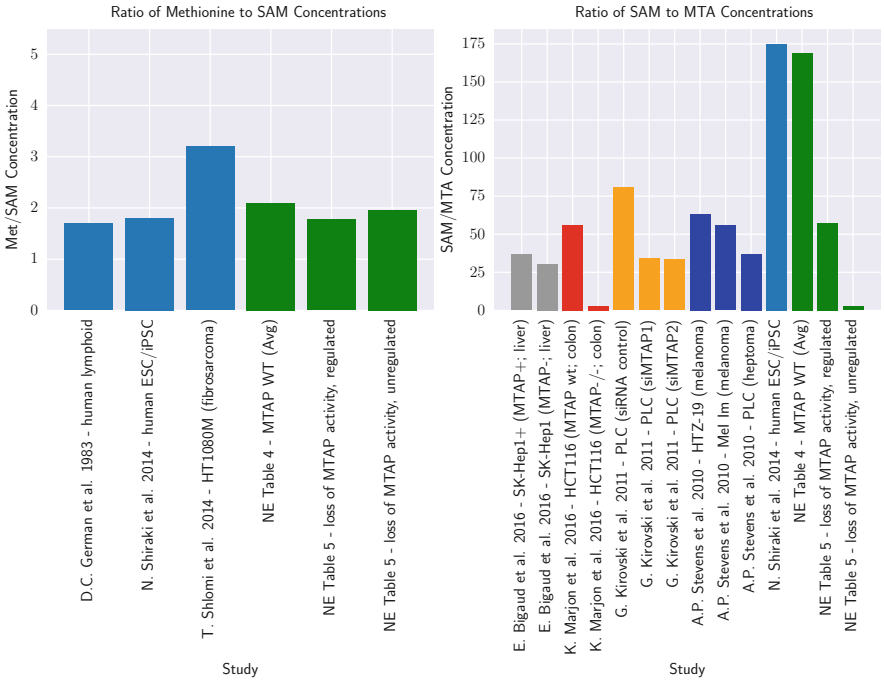

Fig. 3 Comparison between experimental and predicted ratio of equilibrium concentrations between methionine/SAM and SAM/MTA

for several experimental studies. The ratio of methionine/SAM predicted by the Nash equilibrium approach is found to be in good agreement with all studies, in which approximately half of the methionine pool is used toward production of SAM. Interestingly the ratio of SAM/MTA as predicted by the Nash equilibrium approach most closely matches the values reported by Shiraki et al. [11]; Table 4 further shows that the absolute concentrations for SAM and MTA are strikingly close between the predicted and experimental values in that study.

The Nash equilibrium solution in column 2 of Table 4 required 30 outer loop iterations to converge and 0.05 s on a Dell Inspiron laptop using the Lahey-Fujitsu LF95 DOS compiler. The solution shown in column 3 took 38 outer loop iterations and 0.09 s.

2.2 Inclusion of the Key Enzyme S-Methyl-5′-Thioadenosine Phosphorylase (MTAP)

As noted earlier, the enzyme MTAP is deleted in approximately 15% of all human cancers [18] or is reduced in expression in other types of cancer such as HCC. Thus, studying the impact of MTAP activity on the regulation of the methionine salvage

pathway is of great importance. In this work, only binding of MTA to MTAP is considered. See Appendix 2. Correct inclusion of any enzyme must not change the associated chemical equilibrium. When MTAP is added to the previous metabolic pool and regulated at 0.07 µM, the calculated results shown in Table 4 remain the same.

2.3 *Loss of MTAP Activity*

Loss of catalytic activity of MTAP is studied using the Nash equilibrium approach. Loss of enzyme activity can be interpreted in many ways; however, regardless of whether the loss of activity is the result of gene deletion or reduced levels of expression, there is simply less effective (or no) catalytic activity.

Numerous reports have examined the effect of MTAP knock-down or deletions in a variety of cell models, and the results for a number of these studies are summarized in Fig. 3 alongside the predictions for the Nash equilibrium model incorporating loss of MTAP activity (Table 5).

There is a striking resemblance in the decrease in the SAM/MTA ratio between the findings of Marjon et al. [19] for colon carcinoma and the predictions of the Nash equilibrium model (unregulated) in Fig. 3. Furthermore, there are reports that while a loss of MTAP activity does result in a general increase in MTA levels, the levels of SAM are not altered [7]. These findings are consistent with our predictions in which intracellular SAM remains at approximately 50 µM (see Fig. 2 and compare Tables 4 and 5).

Table 5 Loss of MTAP activity in methionine salvage pathway

Species	Pool (nmols)	Regulated (µM)	Unregulated (µM)	Experimental (µM)	Reference number
Glutamate	0.2				
Methionine	0.075	94.47	97.41	100	[17]
KMTB	1				
ATP	2	1323	1327	[1290,1790]	[15]
H^+	1				
Putrescine	0.005	0.090	1.23	[0.05, 0.3]	[15]
MTA	0.25	0.928	20.12	<5	[14]
MTAP	0.015	10.85	7.81		
MTR-1P	0	22.34	20.36		
Adenine[a]	0.01	6.99	158.79	[0.5, 3]	[16]
Oxygen	1				
SAM	0	53.23	49.88	50	[12]
Spermidine	0	3.74	2.49	[0.03, 10]	

[a]Adenine flux regulated at the value given in table

Importantly, our results elucidated a definitive connection between intracellular adenine flux regulation and MTA accumulation within the cell. This claim is supported by the results given in Table 5, which shows numerical results for the methionine salvage pathway using the proposed Nash equilibrium framework for two separate cases—one in which the adenine flux in the pathway is regulated and one in which it is not regulated. In Fig. 3, the results clearly show that when adenine flux is regulated, the value for the predicted ratio of SAM/MTA is in excellent agreement with the hepatoma and melanoma cancer cell models.

According to our predictions, MTA is observed to increase fourfold in concentration under loss of MTAP activity when adenine is regulated (compare Tables 4 and 5) and increases substantially when adenine is not regulated. Experimental studies have reported a sevenfold increase in intracellular MTA levels upon MTAP deletion, resulting in MTA secretion from the cell [13]. However, other studies have also shown markedly higher increases in MTA upon MTAP deletion (e.g., over 20-fold [19]).

In general, when adenine flux in the pathway is not regulated, then:

1. The adenine concentration becomes significantly higher and reaches a level that can slow cell growth [20].
2. There is a 20-fold increase in the concentration of MTA from ~1 to 20 μM.
3. The putrescine concentration increases by an order of magnitude 0.09 to >1 μM.
4. There is a 10% decrease in the concentration of S-methyl-5-thio-D-ribose 1-phosphate (MTR-1P) within the cell.

Figure 4 provides further evidence of the importance of adenine flux regulation within the methionine salvage pathway. Note that for adenine pathway fluxes

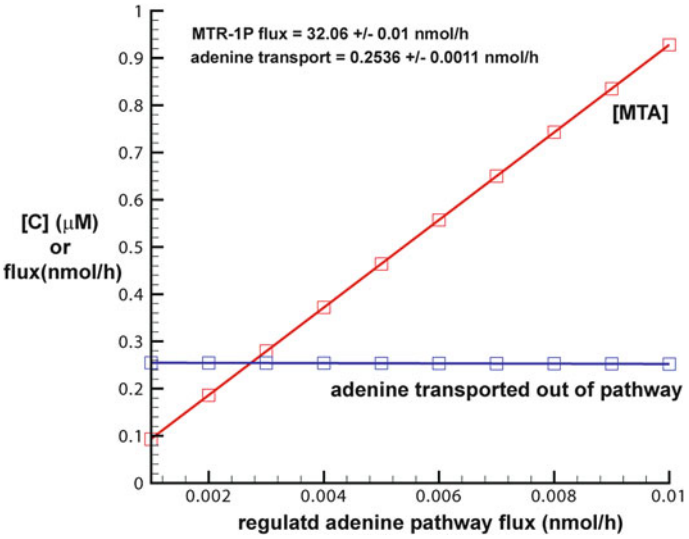

Fig. 4 Impact of regulating adenine flux in the methionine salvage pathway

regulated between 0.001 and 0.01 nmol/h, adenine transport (out of the pathway) remains constant at 0.2536 nmol/h while MTA concentration increases linearly in the range 0.1–1 μM.

Finally, it is important to note that the calculated results shown in Table 5 require very little computational work. Both Nash equilibrium solutions were computed in 20–30 iterations and in less than 0.1 s on a Dell Inspiron laptop.

2.4 Discussion of Methionine Salvage Pathway Results

As noted, many types of cancer cells show loss of MTAP activity, accumulation of MTA, and increased synthesis of the polyamines putrescine and/or spermidine [8]. Nash equilibrium computations performed in this work predict that loss of MTAP activity results in accumulation of MTA, and the level of accumulation is dependent upon whether the adenine flux within the methionine pathway is regulated.

As previously mentioned, some cancers such as hepatocellular carcinoma (HCC) have a loss in MTAP activity rather than complete deletion of the gene. In a study comparing the SAM and MTA levels in melanoma vs. hepatoma cell lines, it was found that the hepatoma line (PLC) exhibited adenine levels that were 56- to 79-fold higher than the melanoma lines [21]! Similarly, in Table 5 it is shown that not regulating adenine in the Nash equilibrium results in a 23-fold increase in adenine concentration. This potentially points to a cancer-specific effect involving adenine (mis)regulation and intracellular MTA accumulation. Furthermore, if the adenine flux is not regulated by the cell, adenine will be overproduced and can result in cell toxicity (e.g., toxic levels of putrescine). Also note that regulation of adenine flux avoids overproduction of polyamines and results in putrescine and spermidine concentrations in the "normal" range, in agreement with data in the Human Metabolome Database (see [15]) and elsewhere.

Interestingly, since adenine is a key metabolite in the rapid regeneration of AMP, cancer cells containing MTAP deletions should be entirely dependent upon de novo purine synthesis of AMP to support growth (rather than the salvage of intracellular adenine pools), which in theory would make them susceptible to inhibitors of this pathway. However, studies have shown that these types of cancer cells resort to salvaging adenine from plasma and adjacent tissues to survive [6], which further complicates the relationship between cancer phenotype and adenine regulation.

3 Conclusions

A Nash equilibrium approach to metabolic pathway modeling, simulation, and analysis was presented. In the first part of this chapter, the Nash equilibrium framework was described and small examples were presented in order to provide a tutorial for the reader. In the second part, the behavior of the methionine salvage

pathway was studied with the intent of demonstrating that the Nash equilibrium framework has the capability to predict metabolic behavior using first principles. Results clearly showed that the Nash equilibrium approach predicts that loss of MTAP activity results in accumulation of MTA and that MTA accumulation is coupled to tight adenine regulation.

Appendix 1

See Table 6.

Table 6 Enzyme-substrate binding energies

Enzyme	Substrate	Binding energy (kJ/mol)
Citrate synthase (4G6B)	Oxaloacetate	−23.01
	Acetyl CoA	−10.37
	NADH	−30.54
Citrate synthase (1OWB)	Oxaloacetate	−23.01
	Acetyl CoA	−10.37
	NADH	−29.29
MTAP	MTA	−29.07

Appendix 2

Methionine salvage pathway biochemical reactions (see Fig. 1).

Reactions Involving Metabolites and Co-factors

$$C_3H_7O_3S^{-1} + C_5H_8NO_4^{-1} \rightleftharpoons C_5H_{11}NO_2S + C_5H_4O_5^{-2} \tag{17}$$

$$C_{10}H_{12}N_5O_{13}P_3^{-4} + C_5H_{11}NO_2S + H_2O \rightleftharpoons HPO_4^{-2} + H_2P_2O_7^{-3} + C_{15}H_{23}N_6O_5S^{+} \tag{18}$$

$$C_{15}H_{23}N_6O_5S^{+} + H^{+} \rightleftharpoons C_{14}H_{24}N_6O_3S^{+2} + CO_2 \tag{19}$$

$$C_{14}H_{24}N_6O_3S^{+2} + C_4H_{14}N_2^{+2} \rightleftharpoons C_{11}H_{15}N_5O_3S + C_7H_{22}N_3^{+3} + H^{+} \tag{20}$$

$$C_{11}H_{15}N_5O_3S + HPO_4^{-2} \overset{\text{MTAP}}{\rightleftharpoons} C_5H_5N_5 + C_6H_{11}O_7PS^{-2} \tag{21}$$

$$\text{(MTR-1P)} \quad C_6H_{11}O_7PS^{-2} \rightleftharpoons C_6H_{11}O_7PS^{-2} \quad \text{(MTRu-1P)} \tag{22}$$

$$C_6H_{11}O_7PS^{-2} \rightleftharpoons C_6H_9O_6PS^{-2} + H_2O \tag{23}$$

$$C_6H_9O_6PS^{-2} + H_2O \rightleftharpoons C_6H_{10}O_3S + HPO_4^{-2} \tag{24}$$

$$C_6H_{10}O_3S + O_2 \rightleftharpoons C_5H_7O_3S^{-1} + CHO_2^{-1} + 2H^+ \tag{25}$$

The overall reaction is given by

$$\begin{aligned} &C_5H_8NO_4^{-1} + C_{10}H_{12}N_5O_{13}P_3^{-4} + C_4H_{14}N_2^{+2} + O_2 \rightleftharpoons \\ &C_5H_4O_5^{-2} + H_2P_2O_7^{-3} + CO_2 + C_7H_{22}N_3^{+3} + C_5H_5N_5 + HPO_4^{-2} \\ &+ CHO_2^{-1} + 2H^+ \end{aligned} \tag{26}$$

and is clearly element and charge balanced.

$$\begin{aligned} \text{MTAP} &= \text{S-methyl-5}'\text{-thioadenosine phosphorylase} \\ \text{MTR-1P} &= \text{S-Methyl-5-thio-D-ribose 1-phosphate} \\ \text{MTRu-1P} &= \text{S-Methyl-5-thio-D-ribulose 1-phosphate} \end{aligned}$$

Key Enzyme-Substrate Reactions

$$\text{MTAP} + C_{11}H_{15}N_5O_3S \rightleftharpoons \text{MTAP} - C_{11}H_{15}N_5O_3S \tag{27}$$

$$\text{MTAP} - C_{11}H_{15}N_5O_3S + HPO_4^{-2} \rightleftharpoons C_5H_5N_5 + C_6H_{11}O_7PS^{-2} \tag{28}$$

Equations (27) and (28) replace Eq. (21) when the enzyme MTAP is included explicitly.

References

1. Lucia, A., DiMaggio, P.A.: A Nash equilibrium approach to metabolic network analysis. In: Pardalos, P., Conca, P., Giuffrida, G., Nicosia, G. (eds.) Machine Learning, Optimization, and Big Data. MOD 2016. Lecture Notes in Computer Science, vol. 10122 (2016). https://doi.org/10.1007/978-3-319-51469-7_4
2. Lucia, A., Thomas, E., DiMaggio, P.A.: On the explicit use of enzyme-substrate reactions in metabolic pathway analysis. In: Nicosia, G., Pardalos, P., Giuffrida, G., Umeton, R. (eds.) Machine Learning, Optimization, and Big Data. MOD 2017. Lecture Notes in Computer Science, vol. 10710 (2018). https://doi.org/10.1007/978-3-319-72926-8_8
3. Lucia, A., DiMaggio, P.A., Alonso-Martinez, D.: Metabolic pathway analysis using a Nash equilibrium approach. J Optim. **71**(3), 537–550 (2018). https://doi.org/10.1007/s10898-018-0605-6
4. Yim, H., Haselbeck, R., Niu, W., Pujol-Baxley, C., Burgard, A., Boldt, J., Khandurina, J., Trawick, J.D., Osterhout, R.E., Stephen, R., Estadilla, J., Teisan, S., Schreyer, H.B., Andrae, S., Yang, T.H., Lee, S.Y., Burk, M.J., Van Dien, S.: Metabolic engineering of Escherichia coli for direct production of 1,4-butanediol. Nat. Chem. Biol. **7**, 445–52 (2011)
5. North, J.A., Miller, A.R., Wildenthal, J.A., Young, S.J., Tabita, R.F.: Microbial pathway for anaerobic 5′-methylthioadenosine metabolism coupled to ethylene formation. Proc. Natl. Acad. Sci. **114**(48), E10455–E10464 (2017)
6. Ruefli-Brasse, A., Sakamoto, D., Orf, J., Rong, M., Shi, J., Carlson, T., Quon, K., Kamb, A., Wickramasinghe, D.: Methylthioadenosine (MTA) rescues methylthioadenosine phosphorylase (MTAP)-deficient tumors from purine synthesis inhibition in vivo via non-autonomous adenine supply. J. Cancer Ther. **2**, 523–534 (2011)
7. Kirovski, G., Stevens, A.P., Czech, B., Dettmer, K., Weiss, T.S., Wild, P., Hartmann, A., Bosserhoff, A.K., Oefner, P.J., Hellerbrand, C.: Down-regulation of methioadenosine phosphorylase (MTAP) induces progression of hepatocellular carcinoma via accumulation of 5-deoxy-5′-methylthioadenosine (MTA). Am. J. Pathol. **178**(3), 1145–1152 (2011)
8. Chang, Y.C., Su, C.Y., Hsiao, M.: Therapeutic targeting of methylthioadenosine phosphorylase. Cancer Cell Microenviron. **3**, e1322 (2016)
9. Kamatani, N., Carson, D.A.: Abnormal regulation of methylthioadenosine and polyamine metabolism in methylthioadenosine phosphorylase-deficient human leukemic cell lines. Cancer Res. **40**, 4178–4182 (1980)
10. Mentch, S.J., Mehrmohamadi, M., Huang, L., Liu, X., Gupta, D., Mattocks, D., Gomez Padilla, P., Ables, G., Bamman, M.M., Thalacker-Mercer, A.E., Nichenametla, S.N., Locasale, J.W.: Histone methylation dynamics and gene regulation occur through the sensing of one-carbon metabolism. Cell Metab. **22**(5), 861–873 (2015)
11. Shiraki, N., Shiraki, Y., Tsuyama, T., Obata, F., Miura, M., Nagae, G., Aburatani, H., Kume, K., Endo, F., Kume, S.: Methionine metabolism regulates maintenance and differentiation of human pluripotent stem cells. Cell Metab. **19**(5), 780–794 (2014)
12. German, D.C., Bloch, C.A., Kredich, N.M.: Measurements of S-adenosylmethionine and L-homocysteine metabolism in cultured human lymphoid cells. J. Biol. Chem. **258**(18), 10997–11003 (1983)
13. Shlomi, T., Fan, J., Tang, B., Kruger, W.D., Rabinowitz, J.D.: Quantitation of cellular metabolic fluxes of methionine. Anal. Chem. **86**(3), 1583–1591 (2014)
14. Henrich, F.C., Singer, K., Poller, K., Bernhardt, L., Strobl, C.D., Limm, K., Ritter, A.P., Gottfried, E., Volkl, S., Jacobs, B., Peter, K., Mougiakakos, D., Dettmer, K., Oefner, P.J., Bosserhoff, A.K., Kreutz, M.P., Aigner, M., Mackensen, A.: Suppressive effects of tumor cell-derived 5′-deoxy-5′-methylthioadenosine on human T cells. Oncoimmunology **5**(8), e1184802 (2016)
15. Wishart, D.S., Jewison, T., Guo, A.C., Wilson, M., Knox, C., Liu, Y., Djoumbou, Y., Mandal, R., Aziat, F., Dong, E., Bouatra, S., Sinelnikov, I., Arndt, D., Xia, J., Liu, P., Yallou, F., Bjorndahl, T., Perez-Pineiro, R., Eisner, R., Allen, F., Neveu, V., Greiner, R., Scalbert, A.:

HMDB 3.0–the human metabolome database in 2013. Nucleic Acids Res. **41**, D801–D807 (2013). https://doi.org/10.1093/nar/gks1065
16. Traut, T.W.: Physiological concentrations of purines and pyrimidines. Mol. Cell. Biochem. **140**, 1–22 (1994)
17. Eagle, H.: Amino acid metabolism in mammalian cell cultures. Science **130**(3373), 432–437 (1959)
18. Beroukhim, R., Mermel, C.H., Porter, D., Wei, G., Raychaudhuri, S., Donovan, J., et al.: The landscape of somatic copy-number alteration across human cancers. Nature **463**(7283), 899–905 (2010)
19. Marjon, K., Cameron, M.J., Quang, P., Clasquin, M.F., Mandley, E., Kunii, K., McVay, M., Choe, S., Kernytsky, A., Gross, S., Konteatis, Z., Murtie, J., Blake, M.L., Travins, J., Dorsch, M., Biller, S.A., Marks, K.M.: MTAP deletions in cancer create vulnerability to targeting of the MAT2A/PRMT5/RIOK1 axis. Cell Rep. **15**(3), 574–587 (2016)
20. Snyder, F.F., Hershfield, M.S., Seegmiller, J.E.: Cytotoxic and metabolic effects of adenosine and adenine on human lymphoblasts. Cancer Res. **38**(8), 2357–2362 (1978)
21. Stevens, A.P., Dettmer, K., Kirovski, G., Samejima, K., Hellerbrand, C., Bosserhoff, A.K., Oefner, P.J.: Quantification of intermediates of the methionine and polyamine metabolism by liquid chromatography-tandem mass spectrometry in cultured tumor cells and liver biopsies. J. Chromatogr. A **1217**(19), 3282–3288 (2010)